

**FABRICATION OF AN ABDOMINAL COMPUTED
TOMOGRAPHY PHANTOM FOR EVALUATION
OF IMAGE QUALITY AND RADIATION DOSE**

ZURAIDA BINTI RAMLI

UNIVERSITI SAINS MALAYSIA

2020

**FABRICATION OF AN ABDOMINAL COMPUTED
TOMOGRAPHY PHANTOM FOR EVALUATION
OF IMAGE QUALITY AND RADIATION DOSE**

by

ZURAIDA BINTI RAMLI

**Thesis submitted in fulfillment of the requirements
for the degree of
Master of Science**

November 2020

ACKNOWLEDGEMENT

In the name of Allah, the Most Gracious and the Most Merciful, all praises to Allah for the strengths and His blessing in completing this thesis successfully.

First and foremost, i would like to express my deepest gratitude to Dr Rafidah Binti Zainon who has supervised my thesis work, with consistent support, guidance, and encouragement that she gave me from the beginning until the completion of this study. Thank you for your most fabulous ideas which had assisted me in completing this thesis. Special appreciation to my co-supervisor, Prof. Dato' Dr Abd Aziz Tajuddin, for his precious technical guidance throughout my study.

Special thanks to my group members Nur Jihan, Nur Diana, and Moayyad, for their help and ideas in completing my laboratory works. I also would like to thank all radiographers at Imaging Unit, Clinical Trial Centre in Advanced Medical and Dental Institute, USM staff for the support throughout the study.

I want to show my gratitude to my beloved family especially my husband, Suhairi bin Mohd Ariffin, my kids, and my parents for their support, patience, pray and concern throughout this study and also thank you to all my colleagues.

I recognise that this research would not have been possible without the financial assistance of P.C.M Sdn. Bhd. (UniKL-RCMP) Academic Staff Higher Education Scheme (ASHES).

Last but not least, thanks also to who had contributed in this study directly or indirectly.

TABLE OF CONTENTS

ACKNOWLEDGEMENT	ii
TABLE OF CONTENTS	iii
LIST OF TABLES	vi
LIST OF FIGURES	vii
LIST OF ABBREVIATIONS	x
LIST OF APPENDICES	xii
ABSTRAK	xiii
ABSTRACT	xv
CHAPTER 1 INTRODUCTION	1
1.1 Background of study	1
1.2 Problem statement	5
1.3 Objectives of study	6
1.4 Thesis outline	7
CHAPTER 2 LITERATURE REVIEW	8
2.1 X-ray interaction with matter	8
2.1.1 Photoelectric effect	10
2.1.2 Compton scattering	11
2.2 Computed tomography	12
2.2.1 Basic principles of CT imaging	14
2.2.2 Material characterisation	20
2.2.3 CT image quality	21
2.2.3(a) Image contrast	22
2.2.3(b) Image noise	23
2.2.3(c) Spatial resolution	25
2.2.3(d) Artifacts	26
2.2.4 CT radiation dose	27
2.2.5 Radiation dosimeter in CT	29
2.3 Abdominal CT phantom	34
2.4 Tissue-mimicking material in CT scanning	35

CHAPTER 3	MATERIALS AND METHODOLOGY	37
3.1	Introduction	37
3.2	Phantom design and development	38
3.2.1	Abdominal CT phantom specification	38
3.2.2	Evaluation of abdominal CT phantom performance	42
3.2.3	Preparation of phantom for CT imaging	44
3.3	Tissue-mimicking materials preparation	47
3.4	Quality control test of a CT scanner	48
3.4.1	Accuracy of CT number	49
3.4.2	Image noise	49
3.4.3	Image uniformity	50
3.5	Thermoluminescence dosimeter (TLD) preparation	51
3.5.1	TLD calibration	52
3.5.1(a)	Annealing procedure	53
3.5.1(b)	TLD irradiation	55
3.5.1(c)	TLD reading	56
3.5.1(d)	Calculation of TLD correction factor	59
3.6	Imaging of an abdominal CT phantom	60
3.6.1	Scanning parameter	60
3.6.1(a)	SECT imaging	62
3.6.1(b)	DECT Imaging	62
3.6.2	Images analysis	63
3.6.3	Radiation dose measurement	65
3.6.4	Optimisation of CT imaging	65
3.6.5	Statistical analysis	66
CHAPTER 4	RESULTS AND DISCUSSIONS	67
4.1	Development of abdominal CT phantom for CT imaging	67
4.2	CT phantom performance	69
4.3	CT scanner quality control tests	72
4.3.1	CT number accuracy	72
4.3.2	Image noise	73
4.3.3	Image uniformity	73

4.4	Thermoluminescence (TLD) calibration	74
4.5	Spectral CT phantom imaging	78
4.5.1	Image quality evaluation	78
4.5.1(a)	CT number evaluation	80
4.5.1(b)	Contrast-to-noise ratio (CNR) analysis	89
4.5.2	Radiation dose assessment	94
4.5.3	Optimisation of CT imaging parameters	103
CHAPTER 5 CONCLUSION AND FUTURE WORK		106
5.1	Conclusion of study	106
5.2	Limitations of study	108
5.3	Recommendations for future work	108
REFERENCES		109
APPENDICES		
LIST OF PUBLICATIONS		

LIST OF TABLES

	Page
Table 3.1 TLD-100 chip characteristic.....	51
Table 3.2 Anneal Protocol for TLD-100.....	54
Table 3.3 The imaging parameters for SECT technique.....	62
Table 3.4 The imaging parameters for DECT technique.....	63
Table 4.1 CT number of water phantom at a central ROI.	73
Table 4.2 Normalised standard deviation of the water phantom at central ROI.....	73
Table 4.3 CT number of water phantom at the periphery ROIs.....	74
Table 4.4 TLDs measurement and calculated correction factor.....	75
Table 4.5 Effective atomic number of tissue-mimicking materials.....	83
Table 4.6 The CNRD values of all tissue-mimicking materials for all imaging parameters.	104

LIST OF FIGURES

	Page
Figure 2.1 Photoelectric effect (Danad <i>et al.</i> , 2015).....	10
Figure 2.2 Compton scattering (Danad <i>et al.</i> , 2015).	11
Figure 2.3 Schematic diagram of the working principles of the CT scan (Tudor <i>et al.</i> , 2014).	15
Figure 2.4 Schematic diagram of CT data reconstruction (Geyer <i>et al.</i> ,2015).16	
Figure 2.5 Schematic diagram for DECT imaging (A) dual-source CT (DSCT), (B) single-source (rapid kVp switching), (C) single- source with two layers detector (Patino <i>et al.</i> , 2016).....	18
Figure 2.6 Material-specific attenuation profile (Patino <i>et al.</i> , 2016).	21
Figure 2.7 Hounsfield scale from -1000 to +1000 (Osborne <i>et al.</i> , 2016).....	23
Figure 2.8 Illustration of simple model for TL and OSL dosimeters.	30
Figure 3.1 Material and methodology.....	37
Figure 3.2 Schematic diagram of a fabricated an abdominal CT phantom.....	39
Figure 3.3 Schematic diagram of the (A) tissue-mimicking materials tube (B) dosimeter insert embedded at the middle of the tissue- mimicking materials tube.	40
Figure 3.4 Schematic diagram of the rubber cap of 6.0 cm cylindrical tube...41	
Figure 3.5 Schematic diagram of the dosimeter’s insert.....	42
Figure 3.6 Single slice scanned developed phantom. The arrow illustrate the position of attenuation profile measurements (A) of phantom for 80 kVp tube voltage and (B) position of attenuation profile for three different material.	44
Figure 3.7 An abdominal CT phantom positioned horizontally on the CT scan couch.	45

Figure 3.8	Schematic diagram of an abdominal phantom set up for scanning	46
Figure 3.9	Equipment for preparation of ferric nitrate and calcium chloride solution.....	48
Figure 3.10	Four ROIs were placed at periphery and one ROI at center on the image obtained for (A) head phantom and (B) abdomen phantom	49
Figure 3.11	50 TLD-100 chips on charging plate.	54
Figure 3.12	Programmable Annealing Oven, LAB-01/400, and the furnace used to anneal the TLD-100 chips.....	55
Figure 3.13	Schematic diagram shows the position of TLDs and ionisation chamber (IC) on CTDI phantom for the calibration process.....	56
Figure 3.14	Schematic diagram of a TLD reader.	57
Figure 3.15	Dymax 5 Charles Austen Pump Ltd.	57
Figure 3.16	Glow curve of TLD plotted on screen.	58
Figure 3.17	(A) Three ROIs (yellow circle) were placing at each tissue- mimicking material area on the image obtained from the scanning (B) Schematic diagram of the distribution of tissue- mimicking material on phantom body.	64
Figure 4.1	A fabricated PMMA abdominal CT phantom with 32.0 cm diameter.....	68
Figure 4.2	A fabricated dosimeter insert (A) TLD slots to place six dosimeters at each scan time (B) cover.....	69
Figure 4.3	Water phantom attenuation profile at different energy level.	70
Figure 4.4	Water phantom attenuation profile for calcium, water and oil.....	71
Figure 4.5	The coefficient of variation (CV%) for the response of each TLD.	77
Figure 4.6	TLD calibration curve.	78
Figure 4.7	Examples of reconstructed images (A) 80 kVp image, (B) 140 kVp image and (C) DECT image.....	79

Figure 4.8	Plot of CT density values of different materials at 80 kVp and 140 kVp.....	81
Figure 4.9	HU measurement for different materials across the image at various kVp, 4.0 mm slice thickness, pitch of 1.2 (A) SECT technique, and (B) DECT technique.....	83
Figure 4.10	Graphs of material-specific attenuation profile at 3,4,5 mm slice thicknesses, 120 kVp, pitch of 1.2 (A) SECT technique, and (B) DECT technique.....	86
Figure 4.11	Graphs of pitch for all tissue-mimicking materials against CT number in (A) SECT and (B) DECT technique.....	87
Figure 4.12	Graphs of CNR against tube voltage for all tissue-mimicking material in (A) SECT and (B) DECT technique.....	90
Figure 4.13	Graphs of CNR against slice thickness for all tissue-mimicking materials in (A) SECT and (B) DECT technique.....	91
Figure 4.14	Graphs of CNR against pitch for all tissue-mimicking materials in (A) SECT and (B) DECT technique.....	93
Figure 4.15	Graphs of radiation dose measured at different tube voltage in (A) SECT technique and (B) DECT technique.....	96
Figure 4.16	Graphs of radiation dose measured against the slice thickness in (A) SECT and (B) DECT technique.....	98
Figure 4.17	Graphs of radiation dose measured against the pitch from (A) SECT and (B) DECT technique.....	100
Figure 4.18	Graphs of radiation dose measured against the pitch at the water material mimicking soft tissue region in SECT and DECT	101
Figure 4.19	Graphs of radiation dose measured for all tissue-mimicking materials against the pitch 0.5 and 1.2 for SECT and DECT.	102

LIST OF ABBREVIATIONS

ALARA	As low as reasonably achievable
AMDI	Advanced medical and dental institute
ART	Algebraic reconstruction technique
BHA	Beam hardening artifacts
CaCl ₂	Calcium chloride
CNR	Contrast-to-noise ratio
CNRD	Dose-weighted contrast-to-noise ratio
CT	Computed tomography
CTDI	Computed tomography dose index
DE	Dual-energy
DECT	Dual-energy computed tomography
DSCT	Dual-source computed tomography
FBP	Filter back projection
Fe (NO ₃) ₃	Ferric nitrate
FOV	Field of view
HU	Hounsfield unit
ILST	Iterative least-squares technique
KERMA	Kinetic energy released in the matter
kVp	Peak kilovoltage
LiF	Lithium fluoride
mA	Milliamperage
PMMA	Polymethyl methacrylate

PMT	Photomultiplier tube
ROI	Region of interest
SD	Standard deviation
SECT	Single-energy computed tomography
SIRT	Simultaneous iterative reconstruction technique
SNR	Signal to noise ratio
TL	Thermoluminescence
TLD	Thermoluminescence dosimeter
TNC	True non-contrast
VMS	Virtual monochromatic spectral
VNC	Virtual non-contrast
VUE	Virtual unenhanced
Z	Atomic number
Z_{eff}	Effective atomic number

LIST OF APPENDICES

- APPENDIX A CT NUMBER OF CALCIUM CHLORIDE, FERRIC NITRATE, WATER AND SUNFLOWER OIL
- APPENDIX B CNR OF CALCIUM CHLORIDE, FERRIC NITRATE, WATER AND SUNFLOWER OIL
- APPENDIX C RADIATION DOSE OF CALCIUM CHLORIDE, FERRIC NITRATE, WATER AND SUNFLOWER OIL

**PEMBIKINAN FANTOM ABDOMEN TOMOGRAFI BERKOMPUTER
UNTUK PENILAIAN KUALITI IMEJ DAN DOS SINARAN**

ABSTRAK

Kebelakangan ini, terdapat beberapa fantom tomografi berkomputer (CT) komersial yang direka untuk pelbagai aplikasi. Bagaimanapun, fantom ini terhad kepada jenis bahan bersamaan tisu tertentu sahaja. Oleh itu, terdapat keperluan untuk membikin fantom abdomen CT yang kos efektif serta mengandungi bahan pelbagai bahan meniru tisu untuk penilaian kualiti imej dan dos sinaran secara serentak. Fantom abdomen CT berdiameter 32.0 sm dibangunkan dengan menggunakan polimetil metakrilat dengan lima set tiub bahan meniru tisu berbentuk silinder dengan diameter 6.0 sm dan sisipan dosimeter pendar kilauterma yang di pasang bersama. Ferik nitrat, kalsium klorida, air, dan minyak bunga matahari masing-masing mewakili darah, tulang, tisu lembut, dan lemak telah digunakan. Fantom telah diimbas pada 80 kVp, 120 kVp, dan 140 kVp dalam CT tenaga tunggal (SECT). Dalam CT dwi-tenaga (DECT), voltan tiub telah ditetapkan pada 80 kVp dan 140 kVp. Pic ditetapkan pada 0.5, dan 1.2 dengan ketebalan kepingan masing-masing ditetapkan pada 3.0 mm, 4.0 mm, dan 5.0 mm. Semua bahan-bahan meniru tisu boleh dibezakan dengan jelas dalam imbasan yang tidak dipertingkatkan. Perbezaan bahan dalam teknik DECT adalah berdasarkan interaksi pelemahan dalam bahan yang disinari. Voltan tiub, ketebalan kepingan, dan pic mempengaruhi kualiti imej dan dos sinaran. Nisbah kontras-kepada-hingar dari DECT memberikan perbezaan yang signifikan dengan SECT untuk semua bahan meniru tisu pada pic 1.2 kerana p-nilai yang diperolehi kurang daripada 0.05. Walaupun dos radiasi yang diperolehi daripada DECT adalah lebih rendah daripada SECT, tetapi

dos sinaran yang direkodkan tidak begitu ketara bagi kedua-dua imbasan kerana p-nilai yang diperolehi lebih besar daripada 0.05. Parameter pengimejan CT yang optimum dari kajian ini boleh digunakan sebagai rujukan untuk pelbagai pengimbasan tisu dalam kedua-dua teknik imbasan

**FABRICATION OF AN ABDOMINAL COMPUTED TOMOGRAPHY
PHANTOM FOR EVALUATION OF IMAGE QUALITY AND RADIATION
DOSE**

ABSTRACT

Recently, there are several commercially available CT phantoms designed for various applications. However, the phantom is limited to certain types of tissue-equivalent materials. Therefore, there is a need to fabricate a cost-effective abdominal CT phantom that contains multi tissue-mimicking materials for image quality and radiation dose evaluation simultaneously. A 32.0 cm diameter abdominal CT phantom was fabricated using polymethyl methacrylate with five sets of cylindrical tissue-mimicking materials tubes with 6.0 cm diameter and thermoluminescence dosimeters slots that attached together. The ferric nitrate, calcium chloride, water, and sunflower oil were used to represent the blood, bone, soft tissue, and fat, respectively. The phantom was scanned at 80 kVp, 120 kVp, and 140 kVp in single-energy CT (SECT). In dual-energy CT (DECT), the tube voltage was fixed at 80 kVp and 140 kVp. The pitch were set at 0.5, and 1.2 and the slice thickness were set at 3.0 mm, 4.0 mm, and 5.0 mm respectively. All the tissue-mimicking materials can be differentiated clearly in an unenhanced scan. The material differentiation in the DECT is based on the attenuation interaction in the irradiated materials. Tube voltage, slice thickness, and pitch affect the image quality and radiation dose. The contrast-to-noise ratio from the DECT gave significant different with SECT for all tissue-mimicking materials at pitch 1.2 as the p-values obtained were less than 0.05. Although the radiation dose measured from the DECT is lower than the SECT, nevertheless the radiation dose from DECT

does not significantly different from SECT as the p-values obtained were greater than 0.05. The optimal CT imaging parameters from this study can be used as a reference for various tissue scanning in both scan techniques.

CHAPTER 1

INTRODUCTION

1.1 Background of study

Computed tomography (CT) is a medical imaging modality that uses narrow X-ray beams which rotates at various angles around the patient to acquire multiple views of the specific body areas. Computer technology will interpret the data to produce cross-sectional views of that body part. Without body cutting, the CT technology allows the user to view organs from outside the body. The CT imaging is based on the attenuation coefficient of radiation that crossing the scanned object, which predominantly by the photoelectric interaction and Compton scattering. The X-ray energy that crossed the scanned structure also interacts with those tissues. The absorption, attenuation, and scattering will occur. The signal arises then detected by a computer system which contains useful information regarding the scanned structure. Lastly, the system will reconstruct an image using that information. Computed tomography is an imaging examination in the medical field that was invented to diagnose any abnormality in human body and also to perform image guided interventions.

The rapid development of technology has led to the existence of the dual-energy CT (DECT) technique since the late 1970s (Riederer and Mistretta, 1977). The DECT technique apply the principle of using high and low energy levels. Nevertheless, the technical limitation has delayed the technology in clinical used. The principle of DECT is it acquire attenuation values of the same structures at two different energy levels, where the name dual arises, that means dual-energy level. The standard energy level used is 80 kVp, and 140 kVp used simultaneously on the same

scanning. By applying two different energies allows the formation of datasets with information regarding tissue composition, providing great information than that available from the single-energy CT (SECT).

In the past few years, the use of DECT in a clinical application has been evaluated. More studies were performed including detection and characterisation of renal stones, kidney neoplasm, lung neoplasm, lymph nodes, and liver. The evaluation in gastrointestinal stromal tumors also studied. Besides, the studies also performed in the evaluation of myocardial and lung perfusion, reduction of metal artifacts, automatic bone removal, and virtual non-contrast imaging also carried out (Henzler *et al.*, 2012).

In order to ensure CT imaging technology is at optimum performance prior used on human, a phantom is a special tool fabricated used to simulate a human tissue in its interaction with radiation. Tissue-equivalent phantom is specifically designed to evaluate the performance and quality assurance (QA) test of CT scanner before it is used on human to ensure that the scanner is at optimum performance. It can be any human structure that contains one or more tissue substitutes. The phantom is used to simulate radiation interactions in the human body. Furthermore, phantoms are also used to assess the effects of imaging parameters to evaluate any information regarding the imaging procedure, such as image quality and radiation dose under condition very close to the real human body.

Phantoms are comprised of materials that must exhibit the same properties relevant to a particular imaging modality as real human soft tissues. The selection of materials in phantom development must have same density and mass attenuation coefficient properties with those human tissues being simulated. The mass attenuation coefficient is defined as the ratio of the linear attenuation coefficient and density of

the absorbing material. It characterises how much radiation penetrated the absorbing material which depends on the density of that material.

Water tank were widely used in radiography experiment due to high accessible, quick and easy to set up. Furthermore, water also is the greatest tissue-mimicking material for soft tissue since it exhibit the closest effective atomic number, absorption coefficients, and mass attenuation as that of the soft tissue being mimicked (Kurudirek, 2017). The used of water tank are still rational in certain experiment until now. Besides, the solid water phantom are used widely. It has very close radiation characteristics comparable to pure water (Hill *et al.*, 2005). The use of tissue-mimicking materials in phantom development is very necessary in enhancing visualisation of the image by simulating required condition possibly encountered in the particular procedure. The tissue-mimicking materials used such as a mixtures of polyurethane, graphite, carbon black and either acetone or isopropanol to represent tissue of head and brain (McDermott *et al.*, 2017), Polymethyl methacrylate (PMMA) (Pauwels *et al.*, 2011; Belinato *et al.*, 2014; Uhrig *et al.*, 2016), poly(glycerol sebacate) (Kossivas *et al.*, 2012), resin (Schindera *et al.*, 2011), ice, modelling wax and ballistic gelatin (Lopes *et al.*, 2018), polyethylene (Matsuda *et al.*, 2012; Abdul Razak *et al.*, 2013), glucose (Li *et al.*, 2014) and nylon (Sookpeng *et al.*, 2016).

The advancement in CT technology has motivated the crucial needs of the phantom to simulate human body to evaluate the performance and quality assurance (QA) test of CT scanner. Besides, the phantoms are often used to study the effect of imaging parameter to image quality and radiation dose. DECT technique requires extra post-processing in image reconstruction. However, the technique does not contribute to additional radiation dose and image quality degradation.

In conventional SECT, the X-ray possess a polychromatic X-ray beams. The lower-energy X-ray will be absorbed by the object rapidly, thus, only the higher-energy X-ray will pass through the object and detected by the scanner. This will contribute to an artifact known as a beam-hardening artifact. The beam-hardening correction is applied to improve the visualisation of the image produced. If the beam-hardening correction is not sufficient, a nonlinear artifact might occur and contribute to image noise.

DECT systems correct this phenomenon, called beam-hardening effective energy shift. DECT images are less affected by beam-hardening artifact by synthesizing virtual monochromatic spectral (VMS) images using dual-energy projection data, thus provide more accurate data than SECT images. Therefore, by applying VMS imaging, the image quality improved by reducing beam-hardening artifacts. VMS images are reconstructed from a pair of accurate material-density images and mass-attenuation coefficients. For a given kiloelectron volt, the object is represented as if it were being imaged with a monochromatic beam at the same voltage. Image noise on VMS images reconstructed from DECT data was significantly lower than SECT. The CNR of VMS imaging also improved by 30% in DECT compared to SECT (Matsumoto *et al.*, 2011; Pessis *et al.*, 2013).

The used of virtual non-contrast (VNC) reconstructions in DECT replaces true non-contrast (TNC) reconstructions in SECT does not contribute to additional radiation dose or penalty to image quality in DECT (Schenzle *et al.*, 2010; Uhrig *et al.*, 2016). In DECT, virtual unenhanced (VUE) images that obtained from contrast-enhanced CT scan will eliminate the need for obtaining separate non-contrast scan before contrast-enhanced CT, potentially reducing the total radiation exposure (Yamada *et al.*, 2014a). Ohana *et al.*, (2014) reported that by applying iterative

reconstruction into DECT, the radiation reduced by over 20%. The radiation dose recorded with DECT technique reported lower compared to SECT technique with good image quality (Forghani *et al.*, 2017).

Several factors affect the image quality and radiation dose in CT scanning. Tube voltage, slice thickness, and pitch affecting the image quality and radiation dose of the image obtained. The CT image quality measured by calculating the contrast-to-noise ratio (CNR). The CNR is associated with the noise, and the contrast inherent in the scanned image. The CNR is proportional to the attenuation value while inversely proportional to the noise on the image. An atomic number of the scanned materials also influence the attenuation value, thus affecting the image quality and radiation dose.

1.2 Problem statement

At present, there are several types of commercially available CT test phantoms for quality control (QC) test, training and research study such as AAPM CT Performance phantom, Catphan phantom, Gammex RMI 467 phantom, semi-anthropomorphic oval thorax phantom (QRM, Moehrendorf, Germany) and American College of Radiology (ACR) phantom. These commercial phantoms are designed for broad markets with specific applications. These phantoms are expensive, costing more than RM 14000 in Malaysia (Universal Medical, 2020). In the event of the phantom is dropped or crashed while handling, especially to those who are new to the field, the user needs to bear the high cost. The propose custom-made CT phantom cost RM 5800 that is much cheaper compared to the commercialised phantom.

The manufactured test phantoms are often considered difficult or tedious to handle and operated. Therefore, the phantoms also have their operational standard that

need to be complied by those who interest to use the phantom. Therefore, these phantoms also not customisable. The available commercialised phantom is limited to certain types of tissue-equivalent materials usually made of polyethylene, polymethyl methacrylate (PMMA), water, and constitute of few tissue-equivalent materials, such as lung, bone, and breast.

Lately, DECT has been undergone remarkable growth as a result of technological advances and new clinical applications (Liguori *et al.*, 2015). DECT also has shown to be a useful imaging modality for the detection of diseases and abnormalities in the human body, Therefore, it is important to determine the patient dosimetry on CT scanners (Sookpeng *et al.*, 2016). The use of CT phantoms is crucial to evaluate the image quality and doses received by the patients. These reasons have been the force behind the efforts to fabricate a practical, convenient and economical phantom that would combine simplicity with quality to evaluate the image quality and radiation dose in abdominal DECT imaging.

1.3 Objectives of study

The main objectives of this study was to develop an abdominal CT phantom for evaluation of image quality and radiation dose.

The specific objectives of this study were listed as follows:

- 1) To design and fabricate an abdominal CT phantom for image quality and radiation dose evaluation in various types of tissue-mimicking materials.
- 2) To compare the image quality and radiation dose obtained from various tissue-mimicking materials using SECT and DECT imaging technique.
- 3) To evaluate the effect of tube voltage, pitch and slice thickness in fabricated CT phantom for determination of optimised image quality and radiation dose.

1.4 Thesis outline

The thesis content is structured as follows:

Chapter 1 provides the details of this study. It discusses the background of the study, problem statement, and objectives of the study.

Chapter 2 presents the literature review related to this study. The principle of the image acquisition in single-energy CT (SECT) and dual-energy CT (DECT) were discussed. Details of the abdominal CT phantom also included in Chapter 2. The literature reviews also discuss other relevant studies on image quality and radiation dose using both SECT and DECT.

Chapter 3 focuses on the materials and methodology related to this study. The phantom development is described in Chapter 3. The technique used to investigate the image quality and radiation dose using SECT and DECT with various imaging parameter is also discussed in Chapter 3.

Chapter 4 focuses on results and discussion on fabricated CT phantom performance test. The evaluation of the tube voltage, slice thickness, and pitch that influences the image quality and radiation dose in SECT and DECT were also discussed.

Chapter 5 summarised the finding of this study. The limitation of the study and the recommendation for future research are listed in Chapter 5.

CHAPTER 2

LITERATURE REVIEW

2.1 X-ray interaction with matter

Attenuation is a process where the incident radiation (photons) is absorbed or scattered as it travels through matter. The degree of attenuation depends on the atomic number, the physical density of the tissue, and the energy of the incident radiation.

The X-ray interacts with matter through five mechanisms; photoelectric effect, Coherent (Rayleigh) scattering, Compton scattering, pair production, and photodisintegration. Photoelectric effect and Compton scattering are the two major ways in the diagnostic X-ray interaction with tissue in the development of image with energy range up to 150 keV (Dance *et al.*, 2014). The pair production is an interaction for higher incident photon energies that greater than 1.02 MeV. An X-ray with less than 1.02 MeV unable to encounter pair production. For photon energy greater than 10 MeV, the photodisintegration will take place. These two interactions does not occur in diagnostic imaging because of their high energy of incident photons (Bushong, 2017). The mechanism of attenuation for CT scanning is dominated by Compton scattering interactions for soft tissue, with some photoelectric effect interactions for materials of higher atomic number(Z). Compton scattering is independent of atomic number. It is proportionally to electron density and inversely to the energy of the incident photon(E). On the other hand, the photoelectric effect is approximately proportional to atomic number and inversely to the energy of the incident photon, $(Z/E)^3$ (Zaccai *et al.*, 2017).

When the X-ray beam travels through the matter, the beam of X-ray is attenuated when photons are absorbed. The interaction of X-ray with matter varies depending on the energy of photons. Photons with higher energy are more capable of travelling (transmitted) through a matter as they have fewer chances of interaction with matter. This is due to the photoelectric effect; the probability of photoelectric absorption is approximately proportional to $(Z/E)^3$, where Z is the atomic number of the tissue atom and E is the photon energy. Thus, an increase in photon energy, E will result in a fast reduce in the interaction of X-ray with the matter.

The importance of photoelectric effect and Compton scattering in diagnostic imaging is associated with a variation of photons absorption by different anatomic structures. The number of X-ray interactions is higher in calcified tissues (e.g., bone) than in soft tissues (e.g., muscle). As a consequence, in soft tissue, more photons in the beam will penetrate the patient while more photon will be absorbed after passing through calcified tissue. This gave contrast to radiograph due to a clear image of calcified and soft tissues.

2.1.1 Photoelectric effect

The photoelectric effect is the process of energy transfer that occurs when ionising radiation interacts with innermost shell electrons of the atom, as shown in Figure 2.1.

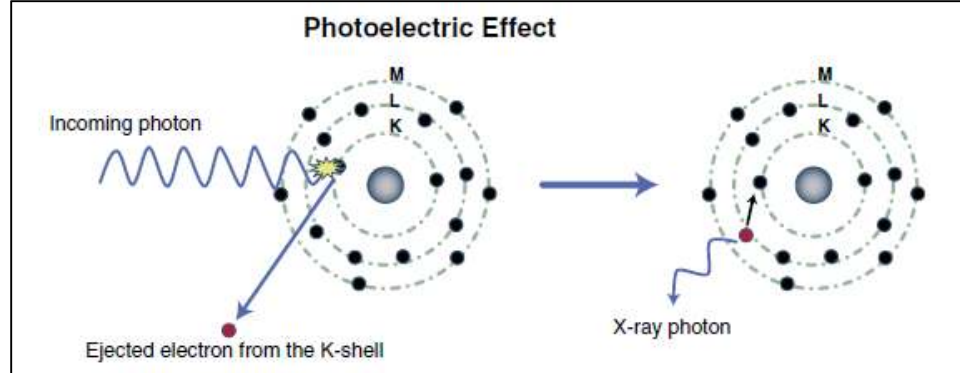


Figure 2.1 Photoelectric effect (Danad *et al.*, 2015).

The innermost shell of the atom is known as K-shell. The X-ray photon energy is totally transfer (absorbed) to the electron, subsequently ionised the atom. Then, the electron eliminated from the atom and becomes a photoelectron. This photoelectron escapes with a kinetic energy that equal to the difference between the energy of the incident X-ray and the binding energy of the electron. The kinetic energy of the photoelectron is shown as Equation 2.1.

$$E_{KE} = E_i - E_b \quad (2.1)$$

Where E_{KE} is the kinetic energy of the photoelectron, E_i is the energy of the incident X-ray, and E_b is the binding energy of the innermost shell electron. The ejection of a K-shell photoelectron by the incident X-ray photon creates a vacancy in the K-shell. This vacancy immediately filled by the electron from the L-shell (outer-shell) with lower binding energy. The emission of X-ray known as characteristic X-ray results from the transition of the electron from L-shell to K-shell. This characteristic X-ray contributes to zero diagnostic information.

The probability of a photoelectric absorption to occur in the matter is dependent on the atomic number of the atom's tissue and the incident photon energy according to $(Z/E)^3$. A photoelectric interaction won't happen except the incident photon has energy equivalent to or greater than the electron binding energy.

2.1.2 Compton scattering

Compton scattering is the interaction between X-ray photon with the outermost shell electrons of the atom, as shown in Figure 2.2. In opposition to the photoelectric effect, the energy of the incident photon not totally absorbed, nevertheless, produce a scattered photon. A portion of the X-ray photon energy is transferred to the scattering electron, consequently ionises the atom and cause an increase in the wavelength of the X-ray. The bombarded electron then ejected from the atom and known as Compton electron. The scattered photons with less energy then travel in all directions. This scattered photons would be travel forward if the energy of incident photon increased. This high energy will result in the greater probability that the angle of the scattered photon will be small; thus, the direction will be almost forward.

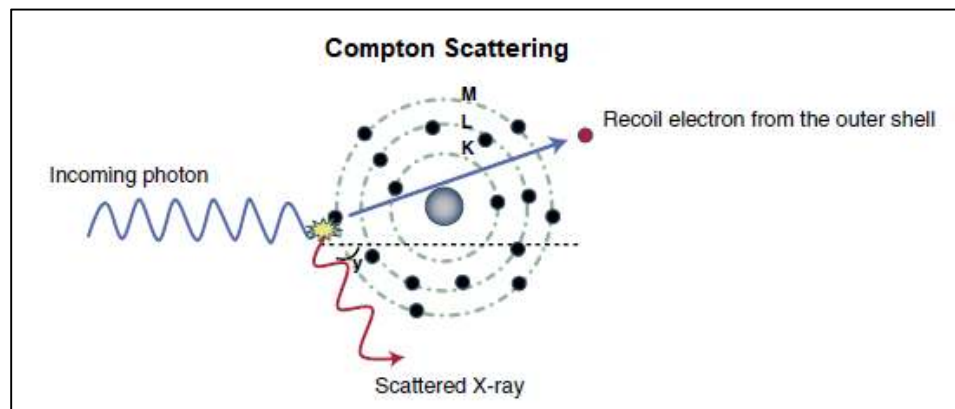


Figure 2.2 Compton scattering (Danad *et al.*, 2015).

The energy of a scattered photon is defined as the relative of the incident photon energy with the electron binding energy and electron kinetic energy as in Equation 2.2.

$$E_S = \frac{E_i}{(E_b + E_{KE})} \quad (2.2)$$

Where E_S is the scattered photon energy, E_i is the energy of the incident photon, E_b is electron binding energy, and E_{KE} is the electron kinetic energy. The energy of the incident photon in Compton scattering interaction is split between the scattered X-ray photon and the Compton electron. The scattered photons darken (fogging/noise) the image, produces zero information because their travel path is changed. The probability of Compton scattering is proportional to the electron density. The number of electrons in bone is higher than in water; thus, the possibility of Compton scattering is identically higher in bone than in tissue.

2.2 Computed tomography

Medical imaging has experienced impressive technological innovation in providing optimum image quality at the lowest radiation dose for diagnostic confidence furthermore improve in the management of patient care. These objectives will be achieved by optimising the technical imaging parameters of the radiographic examination. The discovery of the X-ray was a pioneer by Wilhelm Conrad Roentgen on Friday, November 8, 1895. His discovery revolutionised the modern practice of medicine as well as the world of science.

The conventional radiography has some limitation in ensuring the radiation dose exposed to a patient at acceptable levels without compensating the image quality. The restrictions include an inefficient of X-ray absorption by phosphor crystal in

intensifying screen, which is less than 50%, thus a significant reduction in image information. Other than that, the receptor contrast-latitude trade-off also one of the limitations of conventional radiography. Furthermore, the overlapping which is a fundamental problem in imaging with conventional radiography caused by a radiograph (2D image) is acquired of a 3D object, thus, underneath, and above tissue will be superimposed. This will result in a reduction in conspicuity and lastly, high scatter photon due to broad beam width limits the ability of conventional radiography in ensuring the radiation dose exposed to a patient at acceptable levels in visualising low-contrast tissues (Goldman, 2007a). These limitation overcome by the innovation of tomography technology.

Tomography define as an image of a plane or slice. Tomography operated by moving the X-ray source and the detector at the same time during image formation, thus increased conspicuity through blurring the underneath and above tissues. This technique will obtain the 2D images with minimising overlapping of the structures or tissues. The limitation of tomography is the image quality produced are not satisfactory caused by the interfering objects that just blurred not totally removed from the image, thus interrupt medical diagnosis. In order to resolve this problem, a system that able to reconstruct an image of 2D from a 3D object without interruption or superimpose of other structures in the 3D object was introduced. The reconstruction of the image acquired from projections means the data obtained at various positions and angles. This is the fundamental concept of computed tomography (CT) principles.

In 1972, CT was introduced in the clinical field by Godfrey Hounsfield, a British engineer of EMI Laboratories, England work together with James Ambrose (Geyer *et al.*, 2015). The earliest CT scanner installed by Hounsfield took an extended period (days) in reconstructing a single image from the acquisition of the data until

the image production. The latest multi-slice CT technology has excellent improvements in reconstructing an image from millions of data in a brief period (< second).

The innovation of the CT scanner has significant changes in radiology practice. The improvement contributes to decrease in scanning time with greater anatomy can be examined. The increase in speed will reduce the patient motion, thus, minimise the artifacts, mainly from breathing and peristalsis. In a couple of years, the development of CT scanner technology tremendously expands, especially in dual-energy CT (DECT), spectral CT, and CT molecular imaging (Wu and Shu, 2018).

2.2.1 Basic principles of CT imaging

Computed tomography (CT) imaging is a method of images acquisition through the measurement of the degree of attenuation in tissues of the examined object. Figure 2.3 shows a simple geometry for acquiring a CT image. The X-ray tube and detector are mounted on a rotating gantry that encircling the scanned object. Thus, the projection series (raw data) at multiple angles are produced.

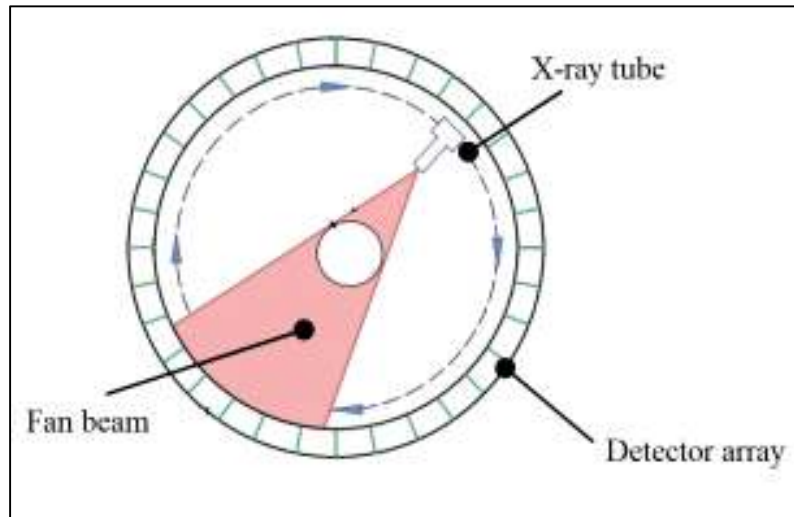


Figure 2.3 Schematic diagram of the working principles of the CT scan (Tudor *et al.*, 2014).

The data acquired from 2D projections then reconstructed to form the 3D CT images. The CT image reconstruction represented in 2D as shades of gray. There are four techniques in CT reconstruction, which is known as CT reconstruction algorithms. The first technique is simultaneous linear equations. The second technique is an iterative techniques that consist of algebraic reconstruction technique (ART), simultaneous iterative reconstruction technique (SIRT), and iterative least-squares technique (ILST). The others techniques in CT reconstruction are filtered back projection (FBP) and lastly the Fourier reconstruction technique. For diagnostic CT, filtered back projection (FBP) is the preferable technique due to its ability to produce high-quality CT images in a short period (Geyer *et al.*, 2015). The data acquisition process for FBP technique to generate the CT image is shown in Figure 2.4.

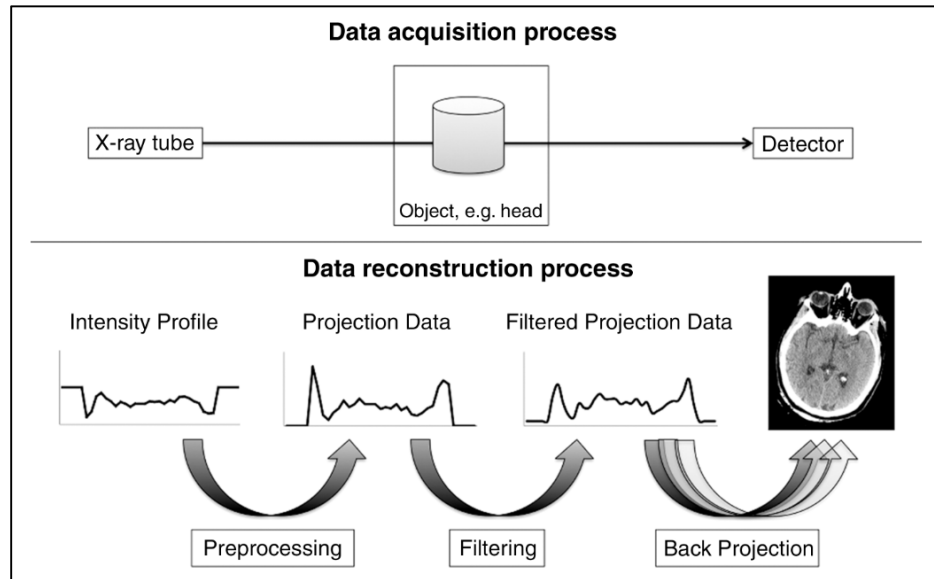


Figure 2.4 Schematic diagram of CT data reconstruction (Geyer *et al.*, 2015).

The basic of CT image depends on the X-ray attenuation when the beam has passed the object. The main interactions are photoelectric effect and Compton scattering. The photoelectric effect mostly relies on photon energy. It related to the atomic number and level of incident photon energy. The Compton scattering does not rely on the photon energy level but associated with the electron density of the bombarded atom. These interactions can be distinguished from two evaluations at discrete energies, which is called as dual-energy (DE) that enable the reduction of the most beam hardening errors.

DECT technology with the first experiment has been performed on the late 1970s (Riederer and Mistretta, 1977) with the concept of using low and high energy levels simultaneously. Nevertheless, technical limitation such as the spatial resolution of the scanner, the unstable CT number and the lengthy scanning time have delayed the technology in used (Millner *et al.*, 1979). In 2006, DECT technique commercially available in clinical used (Zhu *et al.*, 2016).

The success of DECT scanning is depending on the minimal time lapse used between the two acquisitions of the single energy projection. Otherwise, the inconsistencies of the image reconstruction caused by the patient motion that would degrade the accuracies of the image produced, furthermore contribute to image artifact (Goodsitt *et al.*, 2011).

There are some techniques applied in DECT that able to create DECT acquisitions. These techniques vary in the way of low and high energies CT data acquisition with each technology having certain advantages and disadvantages. The technique includes dual-source CT (DSCT) that consists of two X-ray tubes and two corresponding detectors (Figure 2.5A) (Del Gaizo *et al.*, 2014). Tube A covers 50 cm field of view (FOV) while tube B will cover 26.0 cm and 33.0 cm FOV for 1st and 2nd CT generations respectively. The arrangement of X-ray tubes and detectors at an angle of 90° gives advantages to DSCT technique in high temporal resolution. The limitation of DSCT is in data truncation. The scanned object that occurred over the central FOV will cause the raw data in tube B truncated, and the data will have to be extrapolated.

The second types of DECT is a rapid kilovoltage switching uses a single X-ray tube with switching energies illustrated in Figure 2.5B (Del Gaizo *et al.*, 2014). This technology provides fast peak voltage alteration from 80 kVp for low energy to 140 kVp for high energy during a single 360° gantry rotation in as little as 0.25 ms (Silva *et al.*, 2011). The tube current for the two energy settings cannot be adjusted concurrently and remains constant. This limitation will promote in inconsistent noise levels in different kV images. The advantages of rapid kilovoltage switching include an excellent temporal resolution which minimises the potential for motion artifacts. It also provides a 50.0 cm field of view (FOV) for image analysis. The last type of DECT

technology is single-source with two layers detector. This sandwich detector for the first (superficial) layer absorbs low-energy X-ray photons, and the second (deep) layer absorbs high-energy photons (Figure 2.5C) (Del Gaizo *et al.*, 2014). To prevent overlapping of the low and high energy spectra, the K-edge filters are attached to the detectors which produce monochromatic X-ray. The advantage of this technique is, it gives the best spatial resolution and temporal registration. The disadvantage is an increase in the spectral overlap between the low and high energy measurements (Mansouri *et al.*, 2015).

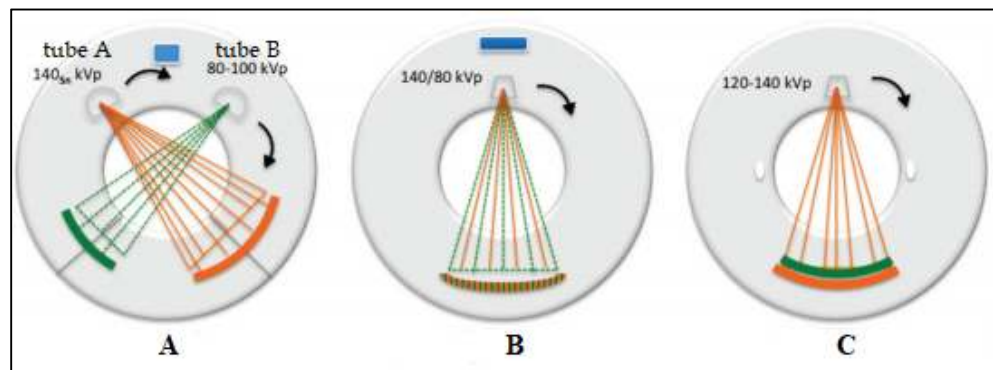


Figure 2.5 Schematic diagram for DECT imaging (A) dual-source CT (DSCT), (B) single-source (rapid kVp switching), (C) single-source with two layers detector (Patino *et al.*, 2016).

The basic principles of DECT are to acquire images using low and high energy usually 80 kVp and 140 kVp simultaneously from the same anatomic part that can be processed for generation of additional datasets. Different energies give a significant effect on the contrast resolution and noise of the two datasets. The low energy (80 kVp) images have superior contrast resolution to high energy (140 kVp) images, nevertheless inferior noise performance (Li *et al.*, 2014). The image produced can be decomposed based on attenuation differences with different in atomic numbers and energies (Aran *et al.*, 2014).

Meanwhile, conventional CT is also known as single-energy CT (SECT) performs scanning with a single polychromatic X-ray beam at tube voltage ranging from 70 to 140 kVp with a standard of 120 kVp that emitted from a single-source and received by a single detector. The inherent contrast of the image reconstructed by CT scanner depends on differences in attenuation of X-ray photon from the various materials in the human body that is soft tissue, air, blood, muscle, calcium, and fat. The attenuation of these materials is dependent on the composition of the tissues; energy level of the incident photon; and the K-edge of that material. Therefore, by changing the level of photon energy, tissue attenuation can be manipulated.

Dual-energy images that acquired from high and low energies will give a significant impact on the contrast resolution and noise. Furthermore, the process of reviewing and presenting the images also quite challenges. To overcome this issue, the dual-energy image data is blended to provide fused images (Apel *et al.*, 2010). The images were transferred to a post-processing workstation (*Syngo* dual-energy software)) to create the fused virtual unenhanced images (Lee *et al.*, 2016). A standard fusing technique using simple linear blending algorithm with blending ratio of 30% 80 kVp data and 70% 140 kVp data that results an image characteristics similar to a standard 120 kVp single-energy image, thus allowing human structures and diseases to be demonstrated (Apel *et al.*, 2010 ; Li *et al.*, 2014).

The application of different energies in DECT techniques gives additional advantages over standard SECT. The benefits of DECT includes any abnormalities obviously demonstrated due to the properties of DECT that have the ability to selectively increase or decrease the reaction of several chemical substances in the body. An example in CT angiography where the blood vessels are highlighted clearly. The other advantage of DECT is the images with and without contrast agents can be

obtained using a single scan instead of two separate scans thus reduce the number of scans further reduce radiation dose to patient. Besides, the DECT can provide information about particular substances in the body due to diseases that can be useful in deciding the correct treatment required and DECT also can significantly improving the image quality of metal that might have been used for joint replacement.

2.2.2 Material characterisation

DECT technique has a potential to distinguish different types of tissues that being scan efficiently than with SECT technique, this process known as material characterisation, material decomposition, material differentiation or material separation. This heightens DECT technique further over standard SECT in clinical applications, in which the aim is to detect the existence of any materials, to characterise the type of the scanned material, and to quantify the amount of a given material (contrast media). DECT enables ascertainment of different material in the body including blood, fat, water, air, bone, and contrast agent based on the attenuation properties that measured in Hounsfield unit (HU) of the materials. This is achievable because each material has different atomic numbers, thus differs in its attenuation profiles through assessing material-specific attenuation characteristic that acquired based on photon spectra generated by high and low energy (Patino *et al.*, 2016; Zhu *et al.*, 2016; Choi *et al.*, 2012).

The effective atomic number (Z_{eff}) will be measured for material that composes from various elements. This Z_{eff} also is considered as a parameter to represent the characteristic of the radiation in different media. Z_{eff} is used to expressing the properties of radiation interaction of material regarding element equivalent and relevant to the irradiated material. Z_{eff} value can be used for the various

energy spectrum of specific ionising radiation because the material with multiple elements has different Z components will resulting in distinct radiation interaction possibility in the diverse energy spectrum (Kurudirek, 2017). The unique attenuation profile by various materials in materials-specific attenuation profile is the basis of DECT material characterisation, as shown in Figure 2.6.

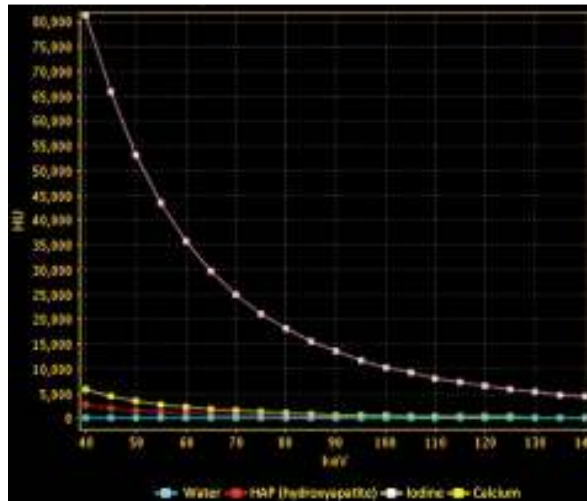


Figure 2.6 Material-specific attenuation profile (Patino *et al.*, 2016).

The material with different atomic numbers will give a difference in CT number that measured in HU will represent a difference in attenuation profile. Thus, the materials can be characterised and differentiated.

2.2.3 CT image quality

CT Image quality deal with the visibility of details the scanned object. High image quality means the anatomical structures, tissues and pathologic lesions are visualise clearly. The strength of CT compared to general radiography technique is its ability to visualise structures of low contrast in a scanned object. The CT images displayed by the different shade of gray for each Hounsfield units. The window width

determines the number of Hounsfield units assigned for each level of gray. The metrics of CT image quality are image contrast, image noise, spatial resolution, and artifacts.

2.2.3 (a) Image contrast

CT image contrast (different brightness) relies on physical contrast and contrast sensitivity. The contrast sensitivity is resulting from the imaging process. This contrast determined by the capability of the CT scanner and methods of the operator in adjusting the window width and window level on the display monitor. Physical contrast, also known as subject contrast. Physical contrast is the contrast inherent in the scanned object that differences in physical density among the tissues, which results in differential absorption of the object. There is a difference in attenuation by X-ray interaction, either absorption or scattering in different types of tissue, consequently providing the differences in X-ray intensity that reaching the detectors (Goldman, 2007b).

CT contrast scale was applied in discussing CT image contrast. The CT number in Hounsfield units (HU) calculated to represent the tissue attenuation using the following Equation 2.3 (Lee *et al.*, 2010; Goldman, 2007b).

$$CT\ number = \frac{\mu_x - \mu_{water}}{\mu_{water}} \times 1000\ HU \quad (2.3)$$

Where μ_x is the linear attenuation coefficient of the target material, and μ_{water} is the water attenuation coefficient. CT number 0 HU is assigned to the density of water. The lowest CT number assigns -1000 HU represents air. Air has the lowest attenuation coefficient; thus, the lowest density compared to other materials. The 1000 HU represents a bone, a dense material. The HU values higher than 2000 assigns very dense materials such as metallic dental fillings (Romans, 2010). The grayscale gives

high-density materials lighter shades of gray, while low-density materials with lower HU values darker shades of gray, as shown in Figure 2.7.

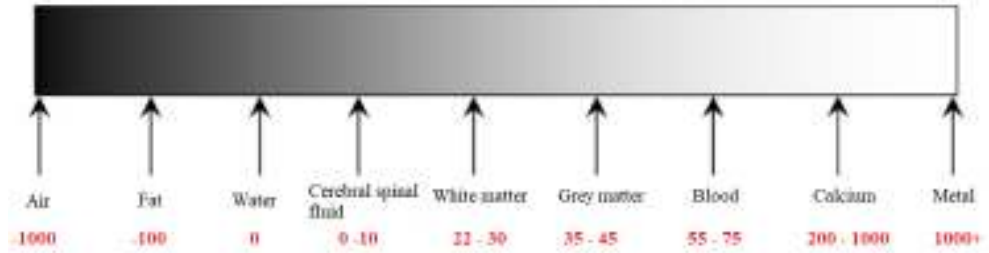


Figure 2.7 Hounsfield scale from -1000 to +1000 (Osborne *et al.*, 2016).

The contrast-to-noise ratio (CNR) is an essential quantity to analyse the detail of the CT image. It quantifies the relation between image contrast and noise. The CNR is calculated follows (Davis *et al.*, 2018) using the formula in Equation 2.4.

$$CNR = \frac{[P_{(Insert)} - P_{(Outside)}]}{\sqrt{\sigma^2_{(Insert)} + \sigma^2_{(Outside)}}} \quad (2.4)$$

Where $\sigma_{(Insert)}$ and $\sigma_{(Outside)}$ are the standard deviations of the ROIs and $P_{(Insert)}$ and $P_{(Outside)}$ are the mean pixel value in a squared ROI inside the tissue-mimicking material insert and the outside the insert in the phantom materials respectively. In principle, any material that supplies with at least two distinctly distinct areas is acceptable for CNR assessment.

2.2.3 (b) Image noise

Image noise is the fluctuation in CT number that occurred in a localised area of the uniform material (IAEA, 2012). Noise appears graininess in the image. Low noise image will presents even to the eye while the high noise image will appear spotty. Image noise was expressed as the standard deviation (σ) of the attenuation

values measured from regions of interest (ROI) that drew in a homogeneous area in the reconstructed image. In the DECT technique, noise measurement was calculated from the weighted-average reconstructed images (Purysko *et al.*, 2014). The CT technique, which is slice thickness, exposure factors, and scan rotation time, affects noise on the image obtained (Goldman, 2007b). Image noise is inversely proportional to CT slice thickness (Alshipli and Kabir, 2017). Increase in slice thickness causes an increase in the number of X-ray photons entering the detector. Therefore, increased in the useful signal detected, consequently, a decrease in image noise.

Furthermore, increasing in tube voltage (kV) causes an increment in some X-ray photon penetrating the target material, then hit the detectors. So, the image noise will decrease as a consequence of an increase in the signal obtained. Abdul Razak *et al.* (2013) concluded that image quality is higher at greater tube voltage with decrease the image noise. The increasing in slice thickness also contribute to high image quality as more photons are produced and captured in the image. In contrary, increasing tube voltage will increase the radiation dose to the exposed material (Goldman, 2007a). The tube current (mA) determines the beam intensity, therefore, determines the number of X-ray photon production. Increase in mA causes more photons reaching the detectors and hence increase the signal intensity, yet reduce noise. Lastly, by increasing the scan time will proportionally increase in image noise. Because, tube current and scan time are tagging together as mAs; thus, the effect is similar (Goldman, 2007b).

The three primary sources that affecting image noise is quantum noise, inherent physical constraints in the system, and reconstruction algorithm (Seeram, 2016). Quantum noise is the major sources that establish noise in the CT image. Quantum noise determined by the number of detected X-ray photons. It is influenced